

Efficient generation of UV-enhanced intense supercontinuum in solids: Toward sub-cycle transient

Cite as: Appl. Phys. Lett. **118**, 261102 (2021); <https://doi.org/10.1063/5.0055348>

Submitted: 28 April 2021 . Accepted: 11 June 2021 . Published Online: 29 June 2021

Yabei Su,  Shaobo Fang, Yitan Gao, Kun Zhao, Guoqing Chang, and Zhiyi Wei



View Online



Export Citation



CrossMark

ARTICLES YOU MAY BE INTERESTED IN

[Demonstration of high efficiency cascaded blue and green micro-light-emitting diodes with independent junction control](#)

Applied Physics Letters **118**, 261104 (2021); <https://doi.org/10.1063/5.0054005>

[Measurement of third-order elastic constants using thermal modulation of ultrasonic waves](#)

Applied Physics Letters **118**, 261903 (2021); <https://doi.org/10.1063/5.0055405>

[Enhancement of A'-site \$Mn^{3+}\$ spin ordering by B-site \$Mn^{4+}\$ substitution in quadruple perovskite \$PbMn_3Cr_3MnO_{12}\$](#)

Applied Physics Letters **118**, 262403 (2021); <https://doi.org/10.1063/5.0051128>



Webinar
How to Characterize Magnetic Materials Using Lock-in Amplifiers

Zurich Instruments MFLI

Zurich Instruments

CRYOGENIC

Register now

Efficient generation of UV-enhanced intense supercontinuum in solids: Toward sub-cycle transient

Cite as: Appl. Phys. Lett. **118**, 261102 (2021); doi: 10.1063/5.0055348

Submitted: 28 April 2021 · Accepted: 11 June 2021 ·

Published Online: 29 June 2021



View Online



Export Citation



CrossMark

Yabei Su,^{1,2} Shaobo Fang,^{2,3,4,a)}  Yitan Gao,^{2,3} Kun Zhao,^{2,3} Guoqing Chang,^{2,3,4} and Zhiyi Wei^{2,3,4}

AFFILIATIONS

¹School of Physics and Optoelectronic Engineering, Xidian University, Xi'an 710071, People's Republic of China

²Institute of Physics, Chinese Academy of Sciences, Beijing 100190, People's Republic of China

³University of Chinese Academy of Science, Beijing 100049, People's Republic of China

⁴Songshan Lake Materials Laboratory, Dongguan, Guangdong 523808, China

a) Author to whom correspondence should be addressed: shaobo.fang@iphy.ac.cn

ABSTRACT

Ultrabroadband generation of white-light continuum spanning from ultraviolet to near-infrared (375–920 nm) is demonstrated by using induced-phase modulation between two-color femtosecond pulses in multiple thin plates. The fundamental wave and its second-harmonic wave from one Ti:sapphire chirped-pulse amplifier are injected into nine 100 μm -thick fused silica plates. When the two pulses are temporally and spatially optimized in the plates, an intense supercontinuum is efficiently achieved by utilizing self-phase modulation and self-steepening together with induced-phase modulation. As a result, using 1 kHz, 1 mJ, and 35 fs pulses at 800 nm as the pump, we demonstrate the generation of 0.6 mJ white-light pulses with an ultra-broad bandwidth supporting 1.6 fs transform-limited pulses corresponding to 0.6-optical-cycle at a central wavelength of 750 nm. Analysis of the calculated spectrum fits the experimental results well, and the pulse is quasi-linearly chirped and compressible. The resulting intense robust supercontinuum could be a promising light source for an ever greater degree of tailored optical waveform coherent control in new parameter spaces.

Published under an exclusive license by AIP Publishing. <https://doi.org/10.1063/5.0055348>

Intense supercontinuum sources have become an enabling tool in many fields such as large-scale imaging of biological dynamics,¹ femtochemistry,² telecommunications,³ sensing, and ultrafast science.⁴ In the past decade, these sources paved the way for the development of high-energy few-cycle pulses, which were widely used in isolated attosecond pulses (IAP) generation allowing to explore the ultrafast dynamics of atomic and molecular physics.^{5–7} Most of the attosecond pulses were generated by the process of high harmonic generation (HHG). The semi-classical three-step model well explains the HHG process,⁸ in which an attosecond pulse originates from half cycle of the electric field of the intense femtosecond driving pulses, and thus, multi-cycle laser driving pulses lead to the attosecond pulse trains. It has been proved that using the sub-cycle pulses with a controllable waveform is more favorable for generating IAPs and can significantly boost the HHG conversion efficiency.^{9,10} Furthermore, the sub-cycle pulses also benefit the study of band structure and electronic dynamics in condensed matter by investigating high-harmonic spectroscopy of solids.¹¹

Besides the generation of over-octave pulses via filamentation and coherent parametric waveform synthesis,^{12–14} another method is a multi-channel compression of supercontinuum from one intense light source based on self-channeling^{15,16} or a gas-filled hollow-core fiber (HCF).^{17,18} However, the high- and near-uniform efficient generation of over-octave supercontinuum¹⁹ is a prerequisite for the synthesis of light fields on a sub-cycle scale. To achieve such supercontinuum, induced-phase modulation (IPM) offers a controllability of the spectral structure by adjusting the intensity ratio and relative time delay between two (or more) input pulses. This approach can generate even broader-band pulses than those produced by only one-color self-phase modulation (SPM).^{20–22} By employing the advantages of IPM in an argon-filled hollow fiber, 1.3-cycle, 2.6 fs pulses with 3.6 μJ energy have been demonstrated by using a 4-f compressor constructed from a spatial light modulator (SLM).²³ To boost the output pulse energy, we already reported 1.7 mJ multi-octave pulses in neon-filled HCF by using IPM, and the output spectrum corresponds to 0.9 fs transform-limited (TL) pulses. Typically, the compression of millijoule-level

pulses in HCFs requires several-meter-long optical arrangements and pressure-gradient technique with a higher overall complexity and daily maintenance operability.²⁴

Recently, a novel technique to broaden spectra in multi-thin plates has been experimentally demonstrated.^{25,26} Unlike HCF that requires a beam-pointing-locking system to prevent fiber head from optically induced damage, this new technique does not need such a complex system and has a high throughput.²⁷ The mechanism of spectral broadening in multi-thin plates is dominated by SPM in the first few plates. For further propagation, the increase in refractive index induced by the pulse makes the velocity of peak gradually slower than the wing of pulse, and the self-steeping begins to play a dominated role and leads to asymmetrical spectral broadening in the last few plates, which has been experimentally proved in our previous work.²⁶ Efforts have been made to achieve transform-limited single-cycle pulses using two-stage compressors.^{28,29} Furthermore, achieving sub-cycle pulses requires even broader supercontinuum. Here, we experimentally present the generation of an IPM-based supercontinuum, corresponding to 1.6 fs (0.6-cycle) transform-limited pulses with 0.6 mJ pulse energy in multi-thin plates. The supercontinuum is generated using two femtosecond pulses centered at two different wavelengths to interact in multi-thin plates. The spectral generation and phase characteristics are investigated by numerical analysis. Thanks to the advanced dispersion management technology to deal with arbitrary spectral phase,^{30–32} the overall spectral phase can be compensated well by using multi-channel compression.^{17,18} We foresee that it can be a promising source for synthesizing high-energy sub-cycle optical waveforms.

The schematic of our experimental setup is shown in Fig. 1(a). A Ti:sapphire chirped-pulse amplifier was used as the front-end source,

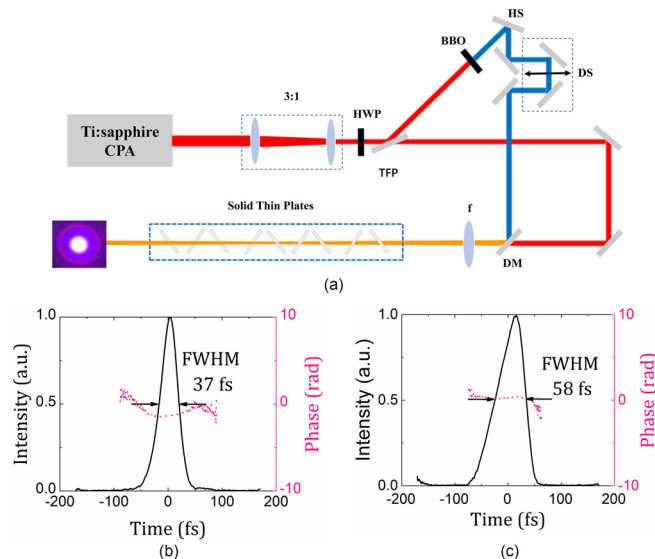


FIG. 1. (a) Experimental IPM setup for supercontinuum generation in fused silica plates. The telescope includes two fused silica lenses: a Plano-convex with $f = 300$ and a Plano-concave with $f = -100$ separated by 200 mm; HWP, half-wave plate; TFP, thin-film polarizer; BBO, β -barium borate crystal with a $200\ \mu\text{m}$ thickness; DM, dichroic mirror; DS, delay stage. The focusing lens $f = 2000$ mm. Temporal profiles (black solid line) and their phases (pink dotted line) of the fundamental pulses (b) and second harmonic pulses (c).

which provided over 1 mJ, 1 kHz, and 35 fs pulses centered at 800 nm. A telescope was used to reduce the beam size from 13 to 4 mm at $1/e^2$ of the intensity profile, such that the overall system could be employed for even higher input pulse energies. Another advantage is that the Rayleigh range at the focus is larger, so the position of the thin plates can be adjusted in a wide tuning range. A half-wave plate (HWP) and a thin-film polarizer (TFP) were used to continuously control the intensity ratio of input pulses. The transmitted pulses with p-polarized through the TFP were used as fundamental pulses (ω). The s-polarized pulses were reflected by the TFP and then converted into second-harmonic pulses (2ω) with a p polarization in a $200\ \mu\text{m}$ -thick, beta barium borate (BBO) crystal. The residual fundamental pulses were fully filtered out by five harmonic separators (HSs). The pulses temporal profile showed a slight distortion due to the walk-off effect in the process of frequency doubling, which was shown in Fig. 1(c). The fundamental pulses and the second harmonic pulses with the same polarization were temporally and spatially recombined by a dichroic mirror (DM) and then were both loosely focused into multiple thin plates for spectrum broadening. The pulses' durations were measured after the DM by a home-made transient-gating frequency resolved optical gating (TG-FROG)³³ and were used for the subsequent numerical calculations. In Fig. 1(b), the fundamental pulse duration was stretched to 37 fs due to the positive dispersion of TFP (144), DM (72), and air ($23\ \text{fs}^2$). The combined beam was focused onto several thin plates by a lens with a focal length of 2000 mm. The thin plates made of fused silica with high optical quality were placed in adjustable holders at the Brewster angle (55.5°). The thickness of each piece is 0.1 (effective thickness of 0.12) and the inner diameter is 10 mm. The input pulses' intensity was set at $10^{13}\ \text{W}/\text{cm}^2$ at the beam waist without any plates. The spectra broadening was optimized for fundamental pulses at first. Assuming that the focus position is $z = 0$. The first plate was placed before the focus at $z = +19$ cm. The rest were placed at $+10, 0, -3, -6, -9, -12, -15, \text{ and } -18$ cm. The principle of placing each plate was for the best stable broadening and long-term operation. Figure 2(a) shows spectrum evolution of fundamental pulses after each plate. The spectrum of apparent asymmetry in the last two plates showed the characteristic of spectral broadening by self-steeping.²⁶ We then added the second-harmonic pulses with about ten percent energy of fundamental pulses to ensure that the plates were not optically damaged. Figure 2(b) shows spectrum evolution at different input power of the second-harmonic pulses. The symmetric spectrum of the second-harmonic pulses indicated that the mechanism of spectra broadening is dominated by SPM because of the much lower input intensity. The temporal and spatial overlap of the fundamental pulses and the second-harmonic pulses was precisely adjusted by using sum-frequency generation in an additional nonlinear crystal and a high-resolution CCD camera.

After optimizing the time delay and the energy ratio between ω and 2ω pulses, the IPM-based supercontinuum was enhanced. The spectra of the input pulses were shown in Fig. 3(a). Figure 3(b) shows the spectra when one of the two beams was blocked. The IPM-based supercontinuum was shown in Fig. 3(c). The input energy of ω pulse was 740, and the output energy was $680\ \mu\text{J}$, corresponding to an efficiency of 85%. The input energy of 2ω pulse was 82, and the output energy was $62\ \mu\text{J}$, corresponding to an efficiency of 76%. The energy in the center part of the beam was above $600\ \mu\text{J}$, corresponding to an overall efficiency of 73%. As shown in Fig. 3(b), a spectral gap from

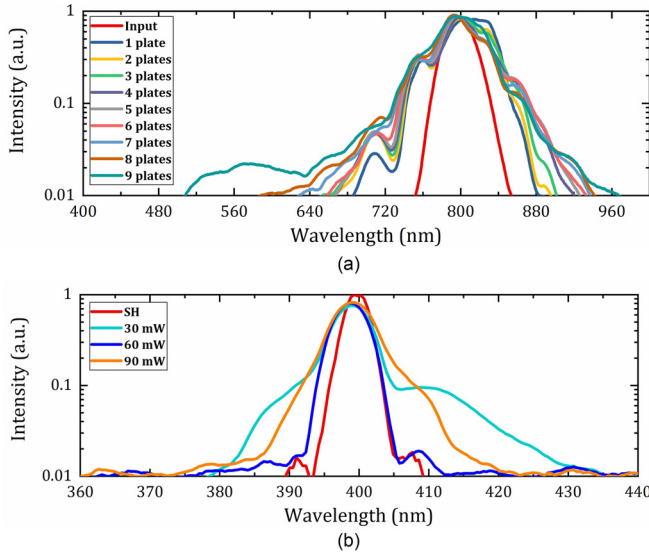


FIG. 2. (a) Spectrum evolution of fundamental pulses after each plate. (b) Spectrum evolution of second-harmonic (SH) pulses at different power.

420 to 500 nm exists between the spectral broadening of ω and 2ω pulses. This proved that IPM is beneficial to enhance the spectral broadening in multiple thin plates. The transform-limited pulse duration and the related calculated electric fields were shown in Fig. 4. The same 1.6 fs full-width-at-half-maxima (FWHM) durations of the main crests of intensity profile were numerically retrieved, corresponding to 0.6 optical cycle at the central wavelength of 750 nm. However, the peak intensity ratios between the highest main field crests and the second highest field crests were 1.4:1, 3.1:1, and 3.7:1.

The intensity profiles of the pulses show the characteristics of the interference of the fundamental with the second harmonic.³⁴ The contrast of the pulses was increased with the extension of spectral

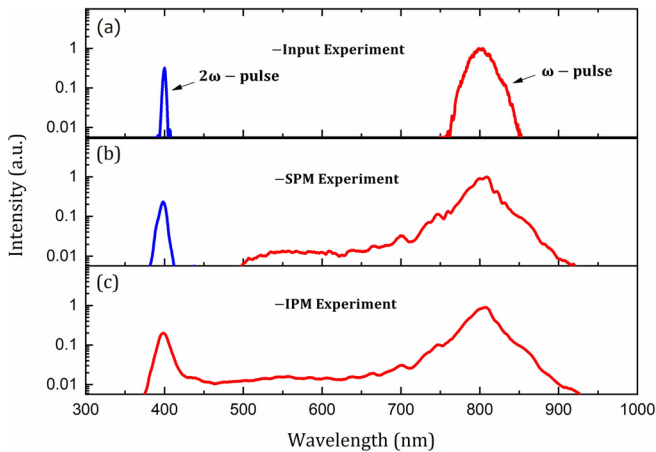


FIG. 3. Experimental results of (a) the spectra of the input fundamental pulses (red line) and the second-harmonic pulses (blue line); (b) the SPM experimental results of the fundamental pulses (red line) and the second-harmonic pulses (blue line); (c) the enhanced IPM results (red).

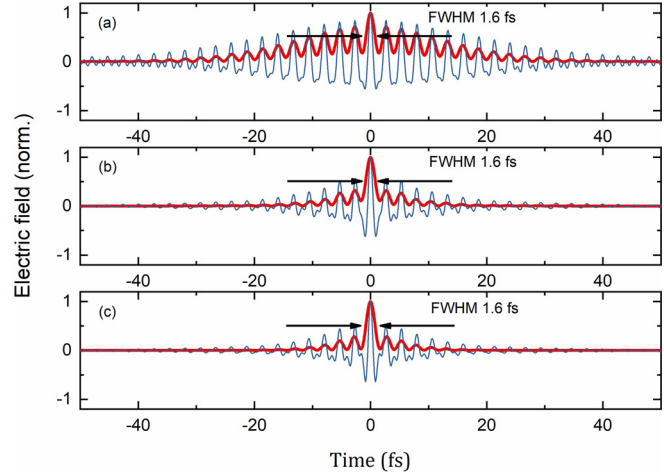


FIG. 4. Calculated electric field (blue line) and intensity profile (red line) of (a) input, (b) SPM, and (c) IPM experiment result. The full width at half maxima (FWHM) durations of their main field are all 1.6 fs. The peak intensity ratios between the main field crests and the second high crests are (a) 1.4:1, (b) 3.1:1, and (c) 3.7:1.

bandwidth. The mechanism of spectral broadening caused by IPM can be well explained by the optical Kerr effect.²⁰ The refractive index of the medium varies with the intensity of the primary pulse whose beam profile is Gaussian shape. As a result, the second harmonic pulses with low energy are phase modulated by the primary fundamental pulse and induced to produce new frequency.

To further understand the experimental results, we performed numerical simulation by solving the following propagation equations:^{35,36}

$$\begin{aligned} \frac{\partial A_1}{\partial z} + i \frac{\beta_{21}}{2} \frac{\partial^2 A_1}{\partial T^2} - \frac{\beta_{31}}{6} \frac{\partial^3 A_1}{\partial T^3} \\ = i \gamma_1 [|A_1|^2 A_1 + \frac{2i}{\omega_0} \frac{\partial}{\partial T} (|A_1|^2 A_1) + 2 |A_2|^2 A_1] \\ - \frac{(i + 1/\omega_0 \tau_c)}{2 \rho_{nt} / \sigma \omega_0 \tau_c} [\rho + \frac{2i}{\omega_0 A_1} \frac{\partial}{\partial T} (\rho A_1)] A_1, \end{aligned} \quad (1)$$

$$\begin{aligned} \frac{\partial A_2}{\partial z} + i \frac{\beta_{22}}{2} \frac{\partial^2 A_2}{\partial T^2} - \frac{\beta_{32}}{6} \frac{\partial^3 A_2}{\partial T^3} \\ = i \gamma_2 [|A_2|^2 A_2 + \frac{2i}{\omega_0} \frac{\partial}{\partial T} (|A_2|^2 A_2) + 2 |A_1|^2 A_2], \end{aligned} \quad (2)$$

where A_j ($j = 1$ or 2) represents the slowly varying amplitude of the fundamental and the second harmonic pulses, respectively, β_{2j} is the group-velocity dispersion (GVD), β_{3j} is the third-order dispersion (TOD), ω_0 is the angular frequency of carrier waves, and τ_c is the characteristic electron collision time. The first term on the right-hand side of the equations contains SPM, self-steepening, and IPM. The last term in Eq. (1) represents the ionization effect, where ρ_{nt} is the total atom density, ρ is the plasma density, and σ is the avalanche cross section. The following equation describes the plasma density:

$$\frac{\partial \rho}{\partial t} = W_I (|A_1|^2) (\rho_{nt} - \rho) + \frac{\sigma \rho |A|^2}{U_i} - \frac{\rho}{\tau_{rec}}, \quad (3)$$

where W_I is the ionization ratio using the Keldysh rate,³⁷ U_i is the bandgap, and τ_{rec} is the recombination time. Since the 2ω pulse has much lower pulse energy, we ignore the ionization effect. The maximum electron density induced by the intense fundamental pulses is $3 \times 10^{24}/\text{m}^3$. In fused silica, the breakdown threshold of electron density induced by femtosecond pulses is $10^{25}/\text{m}^3$.³⁸ It has been proved in hollow fiber that the temporal separation between the two pulses has great impact on the supercontinuum generation. The simulation results of the input pulses and SPM spectra were shown in Figs. 5(a) and 5(b). Here, we assumed the time delay between ω and 2ω pulses in the path of propagation is 187 fs. For the temporal separation of $\tau = -140$ fs at the frontend of the first plate, the simulated supercontinuum was shown in Fig. 5(c), which agrees well with the experimental results. The leading edge of the fundamental pulses interacted with the trailing edge of the second harmonic pulse starting from the first plate, and they met in the last two plates. The set time delay in the thin plates was similar to that in HCF, whose meeting time of the two pulses near the end of the HCF was optimized for supercontinuum generation.²¹ The blue-dashed line in Fig. 5(c) shows the simulated phase of the entire spectrum, and this phase could be well compensated by our custom-designed ultra-wideband chirped mirror pairs³¹ or using commercially available chirped mirrors to compensate the phase of visible to near-infrared wavelength, and using UV-SLM with 4-f system,³² which is a powerful dispersion management device for arbitrary phases compensation (UV-VIS/NIR). Therefore, this millijoule-level supercontinuum could be widely used as the frontend of a high-efficiency compact sub-cycle light source.^{9,39}

In conclusion, we demonstrated the 0.6 mJ white-light generation from ultraviolet to near-infrared in multiple thin plates via two-color IPM effect. We also performed simulation to explain the experiment results and the calculated phase of the spectrum, which shows the compressibility for the sub-cycle pulses. This proves that using two or multi-color fields in solid thin plates is favorable to obtain high-efficiency intense supercontinuum, which could be a versatile source for attosecond science and ultrafast spectroscopy.

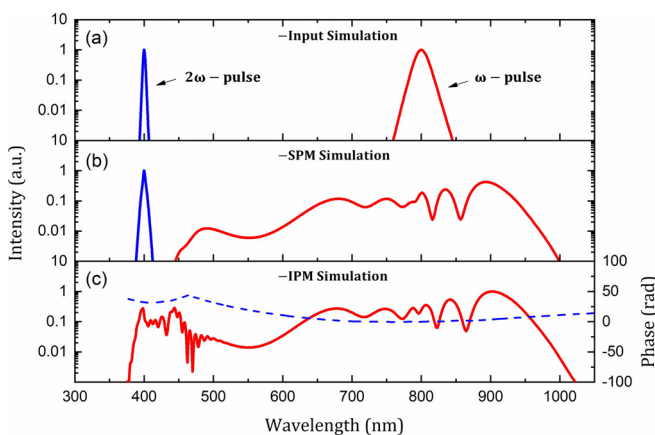


FIG. 5. Simulation results of (a) the spectra of the input fundamental (red line) and the second-harmonic (blue line) pulses; (b) the SPM results of the fundamental (red line) and the second-harmonic (blue line) pulses; and (c) the enhanced IPM results (solid line) and phase (blue-dashed line).

This work was supported by the National Key R&D Program of China (Nos. 2020YFB1313702 and 2017YFC0110301), National Natural Science Foundation of China (Nos. 91950113, 91850209, and 61575219), Scientific Instrument Developing Project of the Chinese Academy of Sciences (No. YJKYYQ20180046), Strategic Priority Research Program of Chinese Academy of Sciences (No. XDB23030203), CAS Key Technology Talent Program (2019), and Youth Innovation Promotion Association CAS (No. 2018007).

We thank Professor Mikio Yamashita and Professor Franz X. Kärtner for many valuable discussions and support.

DATA AVAILABILITY

The data that support the findings of this study are available from the corresponding author upon reasonable request.

REFERENCES

1. J. Fan, J. Suo, J. Wu, H. Xie, Y. Shen, F. Chen, G. Wang, L. Cao, G. Jin, Q. He, T. Li, G. Luan, L. Kong, Z. Zheng, and Q. Dai, *Nat. Photonics* **13**, 809 (2019).
2. Y. Nakano, T. Imasaka, and T. Imasaka, *Anal. Chem.* **92**, 7130 (2020).
3. S. V. Smirnov, J. D. Ania-Castanon, T. J. Ellingham, S. M. Koltsev, S. Kukarin, and S. K. Turitsyn, *Opt. Fiber Technol.* **12**, 122 (2006).
4. A. Dubietis, A. Couairon, and G. Genty, *J. Opt. Soc. Am. B* **36**, SG1 (2019).
5. F. Krausz and M. Ivanov, *Rev. Mod. Phys.* **81**, 163 (2009).
6. M. Hentschel, R. Kienberger, C. Spielmann, G. A. Reider, N. Milosevic, T. Brabec, P. B. Corkum, U. Heinzmann, M. Drescher, and F. Krausz, *Nature* **414**, 509 (2001).
7. T. Gaumnitz, A. Jain, Y. Pertot, M. Huppert, I. Jordan, F. Ardana-Lamas, and H. J. Worner, *Opt. Express* **25**, 27506 (2017).
8. P. B. Corkum, *Phys. Rev. Lett.* **71**, 1994 (1993).
9. G. M. Rossi, R. E. Mainz, Y. Yang, F. Scheiba, M. A. Silva-Toledo, S. Chia, P. D. Keathley, S. Fang, O. D. Mücke, C. Manzoni, G. Cerullo, G. Cirmi, and F. X. Kärtner, *Nat. Photonics* **14**, 629 (2020).
10. E. J. Takahashi, P. Lan, O. D. Mücke, Y. Nabekawa, and K. Midorikawa, *Nat. Commun.* **4**, 2691 (2013).
11. T. T. Luu, M. Garg, S. Y. Kruchinin, A. Moulet, M. T. Hassan, and E. Goulielmakis, *Nature* **521**, 498 (2015).
12. O. D. Mücke, S. B. Fang, G. Cirmi, G. M. Rossi, S.-H. Chia, H. Ye, Y. Yang, R. Mainz, C. Manzoni, P. Farinello, G. Cerullo, and F. X. Kärtner, *IEEE J. Sel. Top. Quantum Electron.* **21**, 1 (2015).
13. A. Alismail, H. Wang, G. Barbiero, N. Altwajry, S. A. Hussain, V. Pervak, W. Schweinberger, A. M. Azzeer, F. Krausz, and H. Fattahi, *Sci. Adv.* **6**, eaax3408 (2020).
14. H. Fattahi, H. Wang, A. Alismail, G. Arisholm, V. Pervak, A. M. Azzeer, and F. Krausz, *Opt. Express* **24**, 24337 (2016).
15. E. Goulielmakis, S. Koehler, B. Reiter, M. Schultze, A. J. Verhoef, E. E. Serebryannikov, A. M. Zheltikov, and F. Krausz, *Opt. Lett.* **33**, 1407 (2008).
16. E. E. Serebryannikov, E. Goulielmakis, and A. M. Zheltikov, *New J. Phys.* **10**, 093001 (2008).
17. A. Wirth, M. T. Hassan, I. Grguras, J. Gagnon, A. Moulet, T. T. Luu, S. Pabst, R. Santra, Z. A. Alahmed, A. M. Azzeer, V. S. Yakovlev, V. Pervak, F. Krausz, and E. Goulielmakis, *Science* **334**, 195 (2011).
18. M. T. Hassan, T. T. Luu, A. Moulet, O. Raskazovskaya, P. Zhokhov, M. Garg, N. Karpowicz, A. M. Zheltikov, V. Pervak, F. Krausz, and E. Goulielmakis, *Nature* **530**, 66 (2016).
19. P. B. Corkum, C. Rolland, and T. Srinivasan-Rao, *Phys. Rev. Lett.* **57**, 2268 (1986).
20. R. R. Alfano and P. P. Ho, *IEEE J. Quantum Electron.* **24**, 351 (1988).
21. N. Karasawa, R. Morita, H. Shigekawa, and M. Yamashita, *Opt. Lett.* **25**, 183 (2000).
22. Y. Yamaguchi, R. Hida, T. Suzuki, and F. Kannari, in *Conference on Lasers and Electro-Optics Pacific Rim* (Optical Society of America, 2017).
23. E. Matsubara, K. Yamane, T. Sekikawa, and M. Yamashita, *J. Opt. Soc. Am. B* **24**, 985 (2007).
24. S. Fang, H. Ye, G. Cirmi, G. M. Rossi, S.-H. Chia, O. D. Mücke, and F. X. Kärtner, in *19th International Conference on Ultrafast Phenomena* (Optical Society of America, 2014), p. 60.

- ²⁵C.-H. Lu, Y.-J. Tsou, H.-Y. Chen, B.-H. Chen, Y.-C. Cheng, S.-D. Yang, M.-C. Chen, C.-C. Hsu, and A. H. Kung, *Optica* **1**, 400 (2014).
- ²⁶P. He, Y. Liu, K. Zhao, H. Teng, X. He, P. Huang, H. Huang, S. Zhong, Y. Jiang, S. Fang, X. Hou, and Z. Wei, *Opt. Lett.* **42**, 474 (2017).
- ²⁷T. Kanai, A. Suda, S. Bohman, M. Kaku, S. Yamaguchi, and K. Midorikawa, *Appl. Phys. Lett.* **92**, 061106 (2008).
- ²⁸M. Seo, K. Tsendsuren, S. Mitra, M. Kling, and D. Kim, *Opt. Lett.* **45**, 367 (2020).
- ²⁹C. H. Lu, W. H. Wu, S. H. Kuo, J. Y. Guo, M. C. Chen, S. D. Yang, and A. H. Kung, *Opt. Express* **27**, 15638 (2019).
- ³⁰O. Razskazovskaya, F. Krausz, and V. Pervak, *Optica* **4**, 129 (2017).
- ³¹S.-H. Chia, G. Cirmi, S. Fang, G. M. Rossi, O. D. Mücke, and F. X. Kärtner, *Optica* **1**, 315 (2014).
- ³²J. Zhu, T. Tanigawa, T. Chen, S. Fang, K. Yamane, T. Sekikawa, and M. Yamashita, *Appl. Opt.* **49**, 350–357 (2010).
- ³³P. Huang, S. Fang, H. Huang, X. Hou, and Z. Wei, *Acta Phys. Sin.* **67**, 244204 (2018).
- ³⁴T. J. Hammond, D. M. Villeneuve, and P. B. Corkum, *Optica* **4**, 826 (2017).
- ³⁵M. Yamashita, H. Sone, and R. Morita, *Jpn. J. Appl. Phys., Part 1* **35**, L1194 (1996).
- ³⁶A. L. Gaeta, *Phys. Rev. Lett.* **84**, 3582 (2000).
- ³⁷L. V. Keldysh, *Sov. Phys. JETP* **20**, 1307 (1965).
- ³⁸Q. Sun, H. Jiang, Y. Liu, Z. Wu, H. Yang, and Q. Gong, *Front. Phys. China* **1**(1), 67–71 (2006).
- ³⁹P. Huang, S. Fang, Y. Gao, K. Zhao, X. Hou, and Z. Wei, *Appl. Phys. Lett.* **115**, 031102 (2019).